ELSEVIER

Computerized Medical Imaging and Graphics 30 (2006) 123–133

Computerized Medical Imaging and Graphics

www.elsevier.com/locate/compmedimag

Reconstruction and rendering of microcalcifications from two mammogram views by modified projective grid space (MPGS)

Chun-Rong Huang [a], Pau-Choo Chung [a], Tong-Yee Lee [b,*], Sheng-Chih Yang [a,d], San-Kan Lee [c]

[a] *Department of Electrical Engineering, Institute of Computer and Communication, National Cheng Kung University, University Road No. 1, Tainan, Taiwan, ROC*

[b] *Department of Computer Science and Information Engineering, National Cheng Kung University, University Road No. 1, Tainan, Taiwan, ROC*

[c] *Department of Radiology, Taichung Veterans General Hospital, Taichung, Taiwan, ROC*

[d] *Department of Electronic Engineering, National Chin-Yi Institute of Technology, Taichung, Taiwan ROC*

Received 21 July 2005; received in revised form 23 November 2005; accepted 21 December 2005

Abstract

Mammograms taken by two views: cranio-caudal (CC) and medio-lateral oblique (MLO) views provide only 2D projections of the microcalcifications, which lack the depth information. Thus, envisioning the relative lesion location from mammograms is a challenge for radiologists. To assist radiologists in locating and rendering lesion tissues, a modified projective grid space (MPGS) scheme is proposed to reconstruct 3D microcalcifications. The MPGS scheme reconstructs 3D microcalcifications in a unique space defined by corresponding points and the epipoles retrieved from the fundamental matrix of the CC and MLO views. Since only corresponding points of images are required in the proposed MPGS scheme, we can avoid the difficulty associated with most reconstruction approaches that require prior complicated calibration of X-ray machine. Considering the deformation of the breast, a new method based on the concept of bundle adjustment is proposed to rectify the 3D locations of reconstructed microcalcifications by uncompressed breast model reconstructed from the real patient body using MPGS scheme with iterative closest point (ICP). Then, the reconstructed microcalcifications are augmented in the real patient body model to show their relative positions.

Keywords: Mammogram; Microcalcifications; Modified projective grid space (MPGS); Bundle adjustment and iterative closest point (ICP).

1. Introduction

Mammogram is one of the most convenient, high accurate and effective breast cancer diagnosis methods for early breast cancer detection. For diagnosis, mammograms are usually taken by two views: cranio-caudal (CC) and medio-lateral oblique (MLO) views. After diagnosis, if the needle biopsy is required, these two views of mammograms are used to provide the basic concept of the lesion locations. However, since each mammogram provides only 2D information, envisioning the relative lesion location, which relies on the radiologists' experiences, is a challenge for radiologists. Therefore, it is common to see that repetitive needle biopsies are conducted for sampling the lesion tissues due to the lack of accuracy in locating mammograms. As a result, patients usually suffer the pain in the procedure due to the repetitive needle biopsies. Thus, a computerized system, which can assist radiologists in accurately locating lesions, particularly 3D positions, is important. Recently, to help radiologists to locate the microcalcifications and tumors in the breast in 3D, Niklason et al. [1] combined multiple views of the breast to reconstruct the 3D information of breast based on tomosynthesis. Maidment et al. [2] presented another approach based on a stereo breast biopsy system from seven views. To remove the requirement of multiple views, Yam et al. [3] presented a novel model-based method for reconstructing the microcalcifications of breast incorporating with a prior geometric model from two mammograms, and they used a number of tissue movement approximations to adjust the compressed breast.

* Corresponding author. Tel.: +886 2757575 62531; fax: +886 6 2747076.

E-mail address: tonylee@mail.ncku.edu.tw (T.-Y. Lee).

0895-6111/$ - see front matter © 2006 Elsevier Ltd. All rights reserved.
doi:10.1016/j.compmedimag.2005.12.003

In this paper, to reconstruct 3D locations of microcalcifications from two mammograms without any prior geometric model or X-ray machine information, we proposed a modified projective grid space (MPGS) scheme [4,5] based on the fundamental matrix [6–8] and pinhole camera system. In MPGS scheme, given any corresponding point pair in two images, the 3D location of the point can be defined uniquely. With this approach, the most frequently encountered difficulties associated with 3D reconstruction of complex calibration can be avoided since only corresponding points of the images in patient's mammograms are required. As we know that mammograms are taken under breast compression, the location of lesions may vary with the pressure of compression applied to the breast. Thus, the reconstructed microcalcifications from the mammograms may misalign with their real positions. To deal with this misalignment problem, a new rectification method based on the concept of bundle adjustment is proposed to adjust the locations of reconstructed microcalcifications by global optimization of the breast alignments between the contours of the real breast model and compressed breast in the mammograms. After the rectification, the microcalcifications are augmented in the real human body model to further demonstrate their relative 3D locations and shapes in the breast. The real human body model is reconstructed based on the proposed MPGS scheme with the iterative closest point (ICP) algorithm [9–11] from several continuous images taken around the patient without prior camera information required. In this part, the ICP algorithm is employed to merge the partial shapes of the human body obtained by MPGS scheme into a whole human body model. Finally, the 3D microcalcification models are augmented on the real human body model according to the ratio of pixel and world coordinate.

In order to accomplish the reconstruction, the 2D locations of microcalcifications in the mammograms should be extracted for the registration of the corresponding microcalcifications in CC and MLO views. Recently, many computer assisted algorithms have been proposed for the detection and the segmentation of microcalcifications from mammograms [12–17]. To solve the problem of microcalcifications detection, in this paper, three modules [18–21] are presented. The first module extracts the breast region from mammograms based on *K*-means clustering-based thresholding. Then, the second module detects suspected regions based on blanket method. The third module extracts the real microcalcifications based on the assumption that the average of gray-level of microcalcifications on the mammograms is generally brighter than that of other tissues. Following the microcalcifications detection is the registration of corresponding microcalcifications in CC and MLO views. However, the registration of microcalcifications is not an easy job, since the breast will be deformed when taking mammograms. Therefore, it is essential to use features that are irrelevant to breast shapes for the registration. In our approach, the gradient code (GC), energy code (EC) and local entropy code (LEC) are applied in order for the registration. According to the result of registration, the 3D locations of microcalcifications can be reconstructed by the modified projective grid space (MPGS).

In the remaining parts of the manuscript, Section 2 describes the detection of microcalcifications. The registration and 3D reconstruction of microcalcifications is presented in Section 3. Section 4 presents the MPGS-ICP scheme in the reconstruction of 3D human breast model from a sequence of patient surrounding images. The rectification of the 3D locations of the microcalcifications based on the real human breast model is proposed in Section 5. Experiments are shown in Section 6. Finally, Section 7 provides the conclusions.

2. Microcalcifications detection

Before the reconstruction of microcalcifications, three modules [18–21] are presented to extract the location of microcalcifications in the mammograms. The first module is designed to extract the breast region from mammograms based on *K*-means clustering-based thresholding method. After breast region extraction, a silhouette of the breast was segmented. The second module refers to the blanket method [22,23] is presented to extract suspected microcalcifications. Let $[(x, y), I(x, y)]$ be the surface area of an object at (x, y) with the gray level $I(x, y)$. The surface area can be estimated by measuring the volume between an upper blanket $U_r(x, y)$ defined by

$$U_r(x,y) = \max\left\{ U_{r-1}(x,y) + 1, \max_{|(s,t)-x,y)| \le 1} U_{r-1}(s,t) \right\} \quad (1)$$

and a lower blanket, $L_r(x, y)$ defined by

$$L_r(x,y) = \max\left\{ L_{r-1}(x,y) - 1, \min_{|(s,t)-(x,y)|\le 1} L_{r-1}(s,t) \right\} \quad (2)$$

where $U_0(x, y) = L_0(x, y) = I(x, y)$ and r is a distance above or below the surface and is a scaling factor of the fractal dimension. The surface area $V(r)$ is defined as follows

$$V(r) = \frac{1}{2} \sum_{(x,y)} \{[U_r(x,y) - U_{r-1}(x,y)] + [L_{r-1}(x,y) - L_r(x,y)]\} \quad (3)$$

Since $V(r)$ is proportional to r, it can be represented as

$$V(r) = k \cdot r^{2-D} \quad (4)$$

Using Eq. (4), we can calculate the fractal dimension D based on log $V(r)$ versus log r as follows

$$D = 2 - \frac{\log V(r) - \log k}{\log r} \tag{5}$$

The volume $V(r)$ is considered as an image surface with the variance specified by the scaling factor r while D can be used as a measure of image texture characterization. To detect the microcalcifications, the properties of high gradients and variances in texture of microcalcifications are considered. In this case, D provides an important indication of the existence of clustered microcalcifications.

To further detect the real microcalcifications from suspected regions, the third module, based on the assumption that the average of gray-level of microcalcifications on the mammograms is generally brighter than that of other tissues, was applied. To avoid the noise, the third module first enhances the low intensity of calcified pixels of microcalcifications by using gradient enhancement. Then, the low contrast of enhanced calcified pixels is improved by using contrast enhancement to reduce the intensities of uncalcified pixels so that the contrast can be increased. Next, to remove and suppress the undesired high intensity pixels of other breast tissues, a Gaussian filter is applied. Finally, entropy-based thresholding [24–27] is applied to obtain the binary image that shows the locations of microcalcifications.

3. Registration and shape reconstruction of microcalcifications

In order to reconstruct the 3D models of microcalcifications, the registration of the microcalcifications between CC and MLO views is required. To achieve the registration, the gradient code (GC), energy code (EC) and local entropy code (LEC) are applied in order. Gradient code captures the changes in gray levels of each detected cluster microcalcifications. The energy code describes the energy of each detected cluster microcalcifications in terms of variance. Local entropy code measures the information contained in each detected cluster microcalcifications.

The gradient code (GC) is calculated by the co-occurrence matrix of the texture of the mammograms. Assume that the gray level range is $G = \{0, 1, \ldots, L-1\}$. Let n_{ij} be the number of transitions made from gray level i to gray level j according to two pixel relative locations. In this paper, we define

$$n_{ij} = \sum_{l=1}^{M} \sum_{K=1}^{N} \delta(l,k) \tag{6}$$

where

$$\delta(l,k) = \begin{cases} 1; & \text{if } (I(l,k) = i \text{ and } I(l,k-1) = j) \text{ or } (I(l,k) = i \text{ and } I(l-1,k) = j) \\ 0, & \text{otherwise} \end{cases} \tag{7}$$

$I(l,k)$ is the gray level of the pixel at location (l,k) and $M \times N$ is the size of the image. From Eq. (6) we define $n = \sum_{i=0}^{L-1} \sum_{j=0}^{L-1} n_{ij}$ where the indices i and j are taken over the gray level range G. The co-occurrence matrix is then defined by $W = \lfloor P_{ij} \rfloor_{i,j \in G}$ where $p_{ij} = n_{ij}/n$. Let τ be the threshold for isolating objects. Thus, the co-occurrence matrix thresholded by τ can be further divided into four quadrants. Since microcalcifications are considered as foreground, the gradient code is defined as follows:

$$\mathrm{GC} = \frac{1}{(L-\tau) \times (L-\tau)} \sum_{i=\tau+1}^{L-1} \sum_{j=\tau+1}^{L-1} |i-j| p_{ij} \tag{8}$$

The energy code describes the energy of each detected cluster microcalcifications in terms of variance. For each $N \times N$ image block described in the registration procedure, let $\boldsymbol{x}_i = (x_{i1}, x_{i2}, \ldots, x_{iN^2})^T$ be the vector corresponding to the ith row vector in the image block. The correlation matrix of the image block can be calculated as $R = (1/N^2) \sum_{i=1}^{N^2} \boldsymbol{x}_i \boldsymbol{x}_i^T$. The energy code is then defined by the largest eigenvalue of R. That is, let $\{\lambda_i\}_{i=1}^{N^2}$ be the eigenvalues of R. Then energy code is obtained as $\mathrm{EC} = \lambda_{\max} = \max_{1 \le i \le N^2} \{\lambda_i\}$.

Local entropy code measures the information contained in each detected cluster microcalcifications. Assume that cluster microcalcifications are information sources as

$$p_{ij}^{\mathrm{FF}} = \frac{n_{ij}}{\sum_{i=\tau+1}^{L-1} \sum_{j=\tau+1}^{L-1} n_{ij}} = \frac{n_{ij}/n}{\left(\sum_{i=\tau+1}^{L-1} \sum_{j=\tau+1}^{L-1} n_{ij}/n \right)} = \frac{p_{ij}}{\sum_{i=\tau+1}^{L-1} \sum_{j=\tau+1}^{L-1} p_{ij}} \tag{9}$$

From Eq. (9) $\{p_{ij}^{\mathrm{FF}}\}_{i \in G_1, j \in G_1}$ forms a probability distribution of foreground to foreground (FF) and its corresponding entropy is given by

$$H_{\mathrm{FF}}(\tau) = -\sum_{i=\tau+1}^{L-1} \sum_{j=\tau+1}^{L-1} p_{ij}^{\mathrm{FF}} \log p_{ij}^{\mathrm{FF}} \tag{10}$$

The local entropy code (LEC) is defined by Eq. (10), i.e. $\mathrm{LEC} = H_{\mathrm{FF}}(\tau^*)$, where τ^* is the optimal threshold generated by entropic thresholding method.

The registration procedure of microcalcifications is performed as follows:

1. Divide images in CC and MLO views into $N \times N$ image blocks with half block size,

2. From each image block, calculate GC, EC and LEC for registration.
3. All image blocks in CC and MLO views are then compared in the priority order of GC, EC and LEC in a binary decision tree.
4. When the decision reaches a tree leaf, each image block in CC and MLO views is prioritized according to these three features.

In our system, after automatic microcalcifications detection and registration, the results can be shown to the radiologists to perform further manual selection of the corresponding microcalcifications between CC and MLO views or directly continue the following reconstruction procedure. From the results of microcalcifications registration, the corresponding image blocks between CC and MLO views are obtained. The corresponding points of images can be easily retrieved from the corresponding image blocks. Based on the corresponding microcalcifications, modified projective grid space (MPGS) scheme [4], which is a 3D reconstruction algorithm from two images without calibration, is presented to reconstruct the 3D model of the microcalcifications. This algorithm is based on the concepts of projective grid space presented by Saito and Kanade [5], and is described as follows. Given two images (Fig. 1), assume that a pixel in the first image is (p, q) and its corresponding point of the second image is (r, s). In the projective grid space, the world coordinate of the image point is then defined as (p, q, r). The camera positions of the two basis views are defined as (p_c, q_c, e_{12r}) and (e_{21p}, e_{21q}, r_c), where (p_c, q_c) and (s_c, r_c) are the centers of the first image and second image, respectively. The e_{12r} here is the r element of epipole in the second image, and (e_{21p}, e_{21q}) is the epipole in the first image. In general, to render the 3D objects in a common graphic library for example OpenGL, the objects' coordinates are required to be in the Euclidean space. However, the projective grid space is not the Euclidean space because the grid in the space is not cubic. Therefore, to make each projective grid closer to cubic

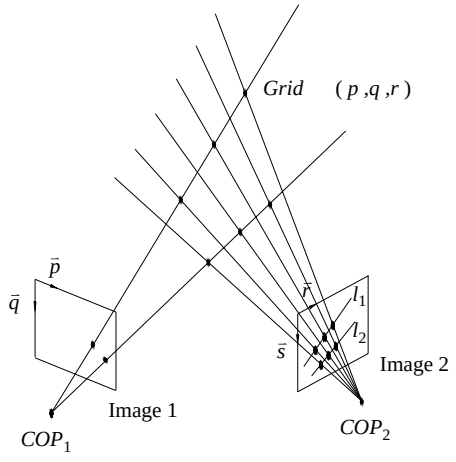

Fig. 1. The projective grid space.

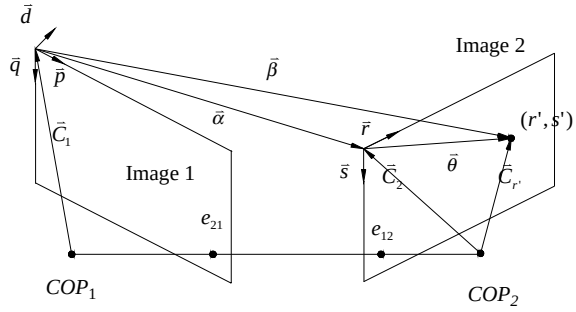

Fig. 2. The modified projective grid space (MPGS).

shape of the Euclidean space, the two basis images are required to be perpendicular to each other. To avoid the restriction of camera position, we propose the modified projective grid space (MPGS) scheme for reconstruction by using a new vector $\vec{d}$ (Fig. 2) that is almost perpendicular to both vectors $\vec{p}$ and $\vec{q}$ in the projective grid space as the z-axis in Euclidean space. The new coordinate system that is composed by $(\vec{p}, \vec{q}, \vec{d})$ is called 'modified projective grid space' (MPGS).

To reconstruct 3D shapes in the MPGS, in Fig. 2, the vector $\vec{\beta}$ is used to find the mapping relation between $\vec{r}$ and $\vec{d}$. For a point (r', s') on the second image, its corresponding $\vec{\beta}$ is equal to

$$\vec{\beta} = \vec{\alpha} + \vec{\theta} = \vec{C}_{r'} + (\mathrm{COP}_2 - \mathrm{COP}_1) - \vec{C}_1 \tag{11}$$

In Eq. (11), $\vec{C}_1$ can be calculated as

$$(e_{21} - \mathrm{COP}_1) = \begin{bmatrix} p_i & q_i & C_{1i} \\ p_j & q_j & C_{1j} \\ p_k & q_k & C_{1k} \end{bmatrix} \begin{bmatrix} e_{21p} \\ e_{21q} \\ 1 \end{bmatrix} \tag{12}$$

The $\vec{C}_{r'}$ will be

$$\vec{C}_{r'} = \begin{bmatrix} r_i & s_i & C_{2i} \\ r_j & s_j & C_{2j} \\ r_k & s_k & C_{2k} \end{bmatrix} \begin{bmatrix} r' \\ s' \\ 1 \end{bmatrix} \tag{13}$$

where C_{2i}, C_{2j}, and C_{2k} can be calculated as follows

$$(e_{12} - \mathrm{COP}_2) = \begin{bmatrix} r_i & s_i & C_{2i} \\ r_j & s_j & C_{2j} \\ r_k & s_k & C_{2k} \end{bmatrix} \begin{bmatrix} e_{12r} \\ e_{12s} \\ 1 \end{bmatrix} \tag{14}$$

With so obtained vector $\vec{\beta}$, the projection proj of $\vec{\beta}$ on $\vec{d}$ is

$$\mathrm{proj} = \frac{\vec{d} \cdot \vec{\beta}}{|\vec{d}|} \tag{15}$$

In this manner, the projection of $\vec{\beta}$ on $\vec{d}$ is treated as the third element of MPGS. From the described derivation, it is clear that the epipoles of two images are required. To calculate the epipoles, the fundamental matrix requires to be calculated by only using corresponding points. Thus, the difficulty associated with the calibration of the X-ray

machine can be avoided. In this manner, all corresponding center points of microcalcification clusters on CC and MLO views are defined uniquely in MPGS. As a result, the MPGS scheme approximates the Euclidean space and each modified grid is treated as the cubic. Since the 3D microcalcifications in two mammograms are reconstructed by MPGS, which is a new space coordinate that can approximate the Euclidean space, the result of the reconstructions can be rendered in any standard graphic library, for example OpenGL, without any transformation. With these center vertices, the 3D locations of the microcalcifications can be obtained.

To further obtain the remaining 3D vertices of the microcalcification clusters in the 3D space, we first take the center $\boldsymbol{C}$ of the microcalcification as the start point. Based on this center $\boldsymbol{C}$, vertices $\boldsymbol{V_i}$, $i=1\ldots m$, around the registration center $\boldsymbol{C}$ of the microcalcification lesions are projected to CC and MLO views, respectively. If the projection of $\boldsymbol{V_i}$ locates at the same corresponding microcalcification blocks on both CC and MLO views, $\boldsymbol{V_i}$ is regarded as a vertex of the microcalcifications. By this approach we can gradually obtain the microcalcification vertices in the 3D positions and therefore, the shape of the microcalcifications. The obtained shape resolution can achieve the accuracy, which is limited only by the digitization resolution.

4. 3D human model reconstruction

Due to the breast compression, the reconstructed microcalcifications would deviate from their real positions. To adjust relative locations of these 3D microcalcifications in the breast, we first reconstruct the real human model from the images of the patient. Then we use the shape of the breast on the real human model to rectify the locations of the microcalcifications. After obtaining the rectified micro-calcifications, we augment and render them to the real human model. To reconstruct the 3D human model, a new algorithm named MPGS–ICP that combines MPGS scheme and iterative closest point (ICP) from multiple images is proposed as follows.

At first, at least eight corresponding points are specified manually between every two neighboring human body images $\boldsymbol{I_i}$, $\boldsymbol{I_{i+1}}$. With these specified corresponding points, the fundamental matrix between two neighboring images can be computed [7]. By using the fundamental matrix, we can find the corresponding epipolar line $\boldsymbol{l_{i+1}}$ on $\boldsymbol{I_{i+1}}$ of the image point $\boldsymbol{x_i}$ on $\boldsymbol{I_i}$. According to epipolar geometry [8], the corresponding point $\boldsymbol{x_{i+1}}$ of $\boldsymbol{x_i}$ that must locate on the corresponding epipolar line $\boldsymbol{l_{i+1}}$, and then $\boldsymbol{x_{i+1}}$ can be obtained by searching the epipolar line $\boldsymbol{l_{i+1}}$. With more corresponding points between two neighboring images, the reconstructed partial shapes of the human body will become more accurate. Since the MPGS-based scheme only reconstructs the partial shape of the object from two neighboring images, the iterative closest point (ICP) [9–11] algorithm, that can perform global and local shape matching, is presented to merge these partial shapes reconstructed by MPGS into a whole object. In the ICP procedure, we define one of the partial shapes as the model shape and its neighboring partial shape as the data shape. The ICP then registers the model shape with the data shape through matching edge information. After the edges of model shape and data shape are matched, we can stitch the data shape with the model shape according to the matched edge. Thus a new shape is obtained by merging these two neighboring shapes (the current data shape and model shape), to represent a larger shape of the real human body. The new shape is considered as a new model shape, and the ICP procedure is repeated to register it with the next neighboring partial shape, which will then be regarded as the data shape. With this procedure, the shape of the whole body can be obtained.

In our approach, the partial shape, which is reconstructed using the images taken from the front side of the patient, is chosen as the initial model shape, while the other reconstructed partial shapes are considered as data shapes. Let the 3D points on the model shape $\boldsymbol{X}$ be represented as $\boldsymbol{X_i}$ ($i=1, 2,\ldots, N_x$) and their corresponding 3D points on the data shape $\boldsymbol{P}$ be $\boldsymbol{P}_i$ ($i=1, 2,\ldots, N_p$). Assume that the transformation from the a data shape point $\boldsymbol{P}_i$ to model shape point $\boldsymbol{X}_i$ is represented as

$$\boldsymbol{X}_i = \boldsymbol{R}\boldsymbol{P}_i + \boldsymbol{T} + \boldsymbol{N}_i \tag{16}$$

where $\boldsymbol{R}$ is a 3×3 rotation matrix, $\boldsymbol{T}$ is a 3×1 translation vector, and $\boldsymbol{N_i}$ is a noise vector. To find the transformation matrices $\boldsymbol{R}$ and $\boldsymbol{T}$ between data and model shapes, the following equation should be minimized

$$\sum_{i=1}^{N} \|\boldsymbol{X}_i - (\boldsymbol{R}\boldsymbol{P}_i - \boldsymbol{T})\|^2. \tag{17}$$

As the correspondences between the continuous images of patient's body are essential to the computation of the transformation $\boldsymbol{R}$ and $\boldsymbol{T}$, ICP algorithm is conducted. Let the distance between the model shape $\boldsymbol{X}$ and a data point $\vec{\boldsymbol{p}}$ on the data shape $\boldsymbol{P}$ be

$$d(\vec{\boldsymbol{p}},\boldsymbol{X}) = \min_{\vec{x}\in X} \|\vec{\boldsymbol{x}} - \vec{\boldsymbol{p}}\|, \tag{18}$$

and $\boldsymbol{Y}$ be the closest points of model shape $\boldsymbol{X}$ and data shape $\boldsymbol{P}$

$$\boldsymbol{Y} = C(\boldsymbol{P},\boldsymbol{X}), \tag{19}$$

where C is the closest point operator. With the closest points $\boldsymbol{Y}$, the least square operation O is computed as:

$$(\boldsymbol{R},\boldsymbol{T},\boldsymbol{d}) = O(\boldsymbol{P},\boldsymbol{Y}) = \min \sum_{i=1}^{N} \|\boldsymbol{Y}_i - (\boldsymbol{R}\boldsymbol{P}_i - \boldsymbol{T})\|^2. \tag{20}$$

The steps of MPGS–ICP algorithm is summarized as follows

1. Assign the projective grid space coordinates of epipoles and camera centers for every two neighboring images.
2. Calculate the vector $\vec{C}_i$ and $\vec{C}_{i+1}$ according to the general pinhole camera model by (12) and (14).
3. Calculate $\vec{\beta}$ of corresponding pixels on the second image and project each $\vec{\beta}$ on $\vec{d}$.
4. Assign the initial model shape X to be the partial shape obtained from the two front images of the patient and pick one of its neighboring partial shapes as the data shape P.
5. Compute the transformation R and T between model shape and data shape using iterative steps
   a. Initialize parameters: $\boldsymbol{P}_0=\boldsymbol{P}$, $\boldsymbol{R}=\boldsymbol{I}$, and $\boldsymbol{T}=0$.
   b. Compute the closest points: $\boldsymbol{Y}_k=C(\boldsymbol{P}_k, \boldsymbol{X})$.
   c. Compute least square solution $(\boldsymbol{R}_k, \boldsymbol{T}_k, \boldsymbol{d}_k)=O(\boldsymbol{P}_0, \boldsymbol{Y}_k)$.
   d. Apply $\boldsymbol{P}_{k+1}=\boldsymbol{R}_k\boldsymbol{P}_0+\boldsymbol{T}_k$.
   e. Compute the mean square error and examine the termination condition. If the mean square error is larger than a threshold value, go to step b; otherwise, terminate the iteration and go to step f.
   f. Overlay the data shape to the model shape according to the transformation and obtain a new model shape.
   g. If all the partial shapes are merged, terminate the procedure. Otherwise, take the next neighboring partial shape as the data shape and go to step 5 to repeat the procedure with the new model shape and the new data shape.

With this algorithm, the entire 3D human body model is reconstructed. The reconstructed 3D human body model, which, as may have been noted, is obtained under uncompressed mode, will be used in the Section 5 as a golden model in the rectification of microcalcifications.

5. Rectifying locations of microcalcifications

As we have learned from Section 3, the microcalcifications are reconstructed from mammograms, which are taken under breast compression. Thus, it is necessary to adjust the locations of the microcalcifications so that the microcalcifications can be restored into its original positions in the breast. In our approach, the concept of bundle adjustment [29,30], which is a standard technique to optimize the 3D structure of points and motion by fitting the 2D image feature correspondences across views, is used to rectify the 3D coordinates of microcalcifications into the coordinates in an uncompressed breast.

We set the view direction of the virtual camera on the CC view, from the top of the breast, on the uncompressed human breast model reconstructed in Section 4. Then, we also set the view direction of the virtual camera on the MLO view, from side view of the breast. From these two viewing directions, we can obtain two images CC_H and MLO_H, respectively. In the following, the contours of the uncompressed breast model from the CC and MLO views can be retrieved from the CC_H and MLO_H. We also retrieved the breast contours from the CC and MLO views of mammograms. Then, for each contour, we first approximate it by polygon line segments. From the polygon line segments, piece-wise correspondences of the breast contours between CC_H and CC pair are obtained. Similarly, we can also obtain the piece-wise correspondences between MLO_H and MLO pair. Then, we adjust the 3D positions (vertices) of the uncompressed breast model and the projection matrices, which are applied to obtain CC_H and MLO_H, by minimizing the distance of the corresponding contour points between CC_H and CC pair and MLO_H and MLO pair simultaneously. Let $\boldsymbol{X}_i$ be the ith vertex of the uncompressed human breast model and $\boldsymbol{P}_{CC_H}(\boldsymbol{X}_i)$ and $\boldsymbol{P}_{MLO_H}(\boldsymbol{X}_i)$ denote the 2D image projection points of $\boldsymbol{X}_i$ in CC_H and MLO_H views, respectively, where $\boldsymbol{P}_{CC_H}(\cdot)$ and $\boldsymbol{P}_{MLO_H}(\cdot)$ are the perspective projection matrices from viewing directions of CC and MLO views of virtual camera. Also let the image points of polygon line segments on the breast contours from the CC and MLO views be represented by u_{CCi} and u_{MLOi}, respectively. The total distance error between the contours of CC_H and CC pair and MLO_H and MLO pair is defined as

$$E=\sum_{i=1}^{N}\omega_i[(u_{CCi}-\boldsymbol{P}_{CC_H}(\boldsymbol{X}_i))^2 + (u_{MLOi}-\boldsymbol{P}_{MLO_H}(\boldsymbol{X}_i))^2], \quad (21)$$

where $\omega_i=1$ when the projection of the ith vertex is on the contour, and $\omega_i=0$, otherwise. The minimization is executed by the iterative non-linear Levenberg–Marquardt optimization algorithm [31]. After the minimization, the new positions of the 3D breast model and the new projection matrices to obtain CC_H and MLO_H views can be computed. Applying the new projection matrices on the new 3D breast model, we can obtain new CC_H and MLO_H images. From the new CC_H and MLO_H, the contours of the 3D breast model from the CC and MLO views can be retrieved. Then, we approximate the new contours by line segments again and repeat the same procedure mentioned above until the distance error E is smaller than a threshold value. According to the procedure, the corresponding image projection of the original 3D human breast model on the mammograms can be obtained. We then consider those spaces (points or voxels) in the original 3D human breast model whose image projections are within the same registered microcalcifications regions on both CC and MLO mammograms as the microcalcifications. As the projection could be conducted on any coordinate values, it should be noted that the resolution of the points in the 3D human breast model should not be limited by any constraint except by the resolution in the microcalcifications. Thus, the 3D positions of the microcalcifications and their shapes in the uncompressed breast can be obtained.

As it might have been noted that our approach requires two views to reconstruct the locations of microcalcifications. However, this limitation should not significantly hinder its applicability. In general, when a microcalcification cluster is identified in one view, it should be also identified in the other view. If the microcalcification cluster is not identified in the other view, the microcalcifications may be so close to the chest wall not to be able to pull out for making the film or the patient could not tolerate the filming due to hurt for the procedure. As the density of the subtle microcalcification cluster is very similar to the glandular tissue, under exposure of the film or increased density of the breast parenchyma might also cause difficulty in detection of the microcalcifications. However, these problems could be solved by readjustment of the exposure condition or appropriate compression to the breast tissue. In [32], Hackshaw et al. revealed that in 23 of the 110 women, the breast cancer was missed in one view and only two were not visible on the oblique view. It also indicated that cancers missed using a single oblique view tended to be smaller and lacked microcalcifications. Therefore, in breast cancer with microcalcifications, when compared with the detection between one view and two views, less misdiagnosed cases are found from two view mammograms.

6. Experiments

In the experiment of microcalcifications registration, 15 pairs of CC and MLO views from Taichung Veterans General Hospital were used for evaluation. All these cases are specially selected such that the lesions can be visible from ultrasound. To test the proposed registration methods, we used mutual evaluation method to register microcalcifications from CC to MLO views and from MLO to CC views. Thus, the number of evaluation pairs is 30. In these 30 evaluation pairs, only one pair was miss-matched. That is, in one microcalcification pair, from the CC view to MLO view, the corresponding microcalcifications were identified correctly, but from MLO view to the CC view, the corresponding microcalcifications could not be identified. As a result, the correct registration accuracy of our proposed registration method achieved about 96.7% (29/30). Fig. 3(a) and (b) show the example mammograms containing two groups (A and B) of clustered microcalcifications marked in CC and MLO views, respectively. Fig. 4 shows an example of the corresponding results after the registration. The corresponding microcalcifications of the CC view are marked in the grids of the MLO view. Based on the registration results, the two groups of clustered microcalcifications can be localized in a 3D visualization space by MPGS.

In order to evaluate the accuracy of the proposed method, both artificial phantoms and comparisons with ultrasound position reports were performed. In the experiments, artificial phantoms were made by using soft silica gel to simulate the soft tissue of the human breast. Several groups of metals were inserted into the phantoms to represent the locations of the microcalcifications in phantoms. The real positions of the inserted metals were considered as the ground truth of the locations of the microcalcifications in the experiments. Then, we captured the mammograms of the phantoms. From the mammograms of the phantoms, the metals in the phantoms were detected and registered. To further consider the deformation of the phantoms during snapping, the rectification method proposed in our paper was applied. In the rectification, we first projected the uncompressed breast model on the mammogram of the phantom, represented by black contour in Fig. 5, and obtain the initial contour of the uncompressed breast, as shown in cyan in Fig. 5(a), according to the virtual camera. To adjust the uncompressed breast model, we used the constraint Eq. (21) to modify the shape and projection matrix of the virtual camera so that the cyan contour can approach the black

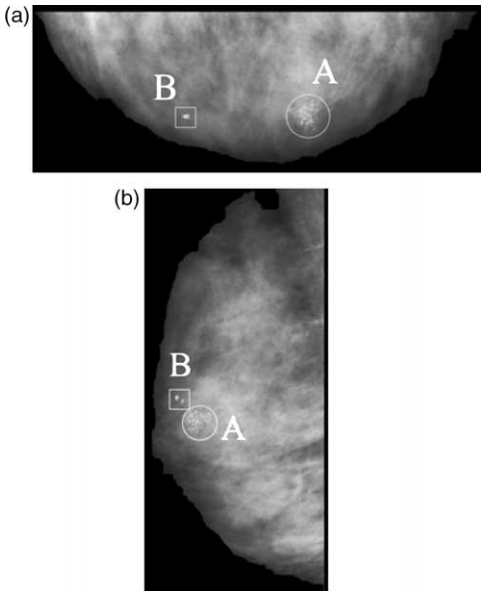

Fig. 3. Mammograms used for registration test. (a) A CC view; (b) an MLO view.

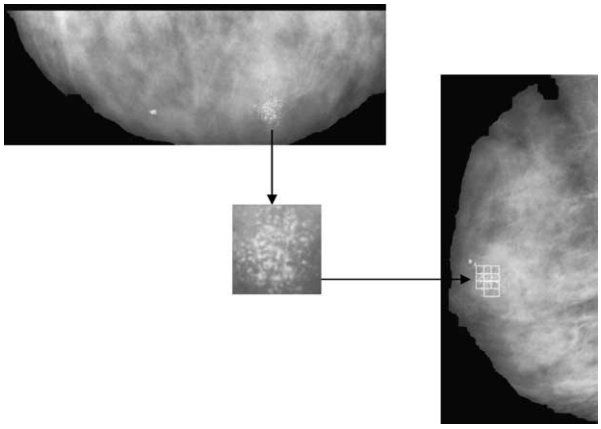

Fig. 4. Final result of registration.

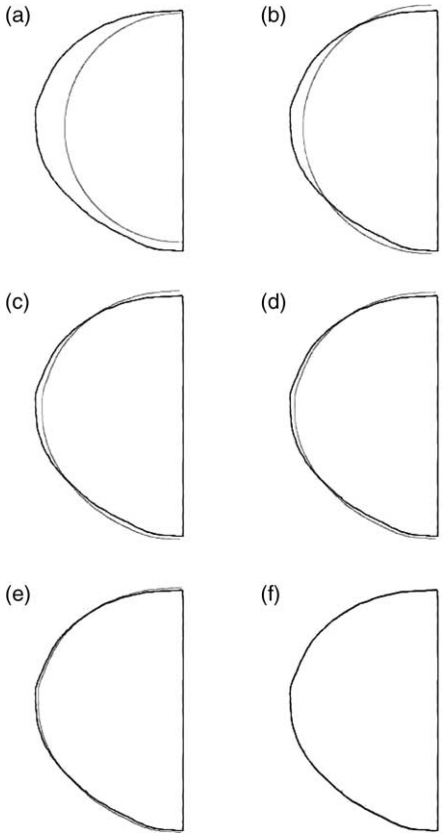

Fig. 5. The deformation results during the rectification in adjusting the contour of the real breast model to fit the breast contour in the mammograms, where the cyan curve represents the contour of the uncompressed model and the black curve represents the contour of the compressed breast in the mammograms. (a) Shows the initial contour; (b)–(e) are the results of 33, 89, 121, 139 iterations and (f) shows the final result.

contour. Fig. 5(a)–(f) show the optimization steps from the uncompressed phantom to the compressed phantom. Table 1 shows the obtained center positions of the microcalcifications after rectification. For comparison, the reconstructed center positions without rectification are also listed. The 'error' in Table 1 is defined as the Euclidean center distance between the ground truth position and the reconstructed position. Without adjustment, the center positions of the microcalcifications by the MPGS scheme are around 4–8 mm. After the adjustment, the errors are decreased to about 2 mm. In clinic, the tissue specimen from microcalcifications, which has to be removed, is bigger than 5 mm in size generally. In this case, our method can perform the sufficient accuracy to assist the surgeon in removing the tissue.

The evaluation of lesion localization is also performed by comparison with the position reports from ultrasound on the same 15 patients. The positions of tumors and clustered microcalcifications of these patients were confirmed in the surgery operations and by ultrasound scanning, which is a traditional approach for identifying the locations of masses before biopsy. Before surgery, these patients also went through mammogram screening with 0.1 mm/pixel resolution. Thus, both the locations detected by ultrasound scanning and the proposed 3D reconstruction method can be obtained. In clinic, to provide reference locations of tumors discovered during ultrasound scanning, the radiologists use quadrants to locate tumors from ultrasound scanning. Although such an approach provides only 2D information of tumors, it can still provide the radiologists the rough locations of tumors when performing needle biopsy. Since we cannot accurately obtain the 3D locations of tumors in the breast for ground truth, we performed orthographic projection of our reconstructed results on the 2D quadrants and compared projection results with results from ultrasound scanning. Complying with the approach used in the ultrasound report, the breast region is divided into 24 quadrants with the nipple as the center. Based on our algorithm, all the reconstructed tumors and clustered microcalcifications are located at the same positions as those obtained from ultrasound scanning. Fig. 6 shows the locations of reconstructed clustered microcalcifications (red) and the positions of the clustered microcalcifications (blue) from ultrasound scanning, from four typical cases for comparison. Please note that our reconstructed algorithm not only provides 2D information as ultrasound provides, but also 3D locations of tumors and microcalcifications in the breast.

Figs. 7 and 8 show the examples of reconstructed microcalcification clusters from various perspective views. Our reconstruction method obtained all the vertices of the microcalcifications by projecting the neighboring vertices of the center to the CC and MLO views. Those vertices, whose projections locate on the microcalcifications in CC and MLO views, were considered as the vertices of the microcalcifications. Then a sphere is used to represent a vertex of the microcalcifications, as shown in Figs. 7 and 8.

Table 1
The estimation results of the positions of microcalcifications in phantoms by MPGS and MPGS with bundle adjustment

Image no.	Real position (mm)	MPGS		MPGS with bundle adjustment	
		Pos. (mm)	Error (mm)	Pos. (mm)	Error (mm)
R01	(−10, 18, 25)	(−10, 14, 27)	4.47	(−9.9, 16.8, 25.5)	1.30
R02	(17, −16, 31)	(21, −18, 34)	5.39	(18.5, −16.7, 32.3)	2.10
R03	(−40, −42, 43)	(−36, −39, 43)	5.00	(−38.2, −40.9, 42.9)	2.11
L01	(15, 7, 12)	(14, 13, 17)	7.87	(14.3, 8.7, 13.5)	2.37
L02	(19, 15, 27)	(19, 18, 22)	5.83	(19.1, 16.4, 25.5)	2.05
L03	(5, −23, 41)	(6, −16, 40)	7.14	(5.2, −20.6, 41)	2.41

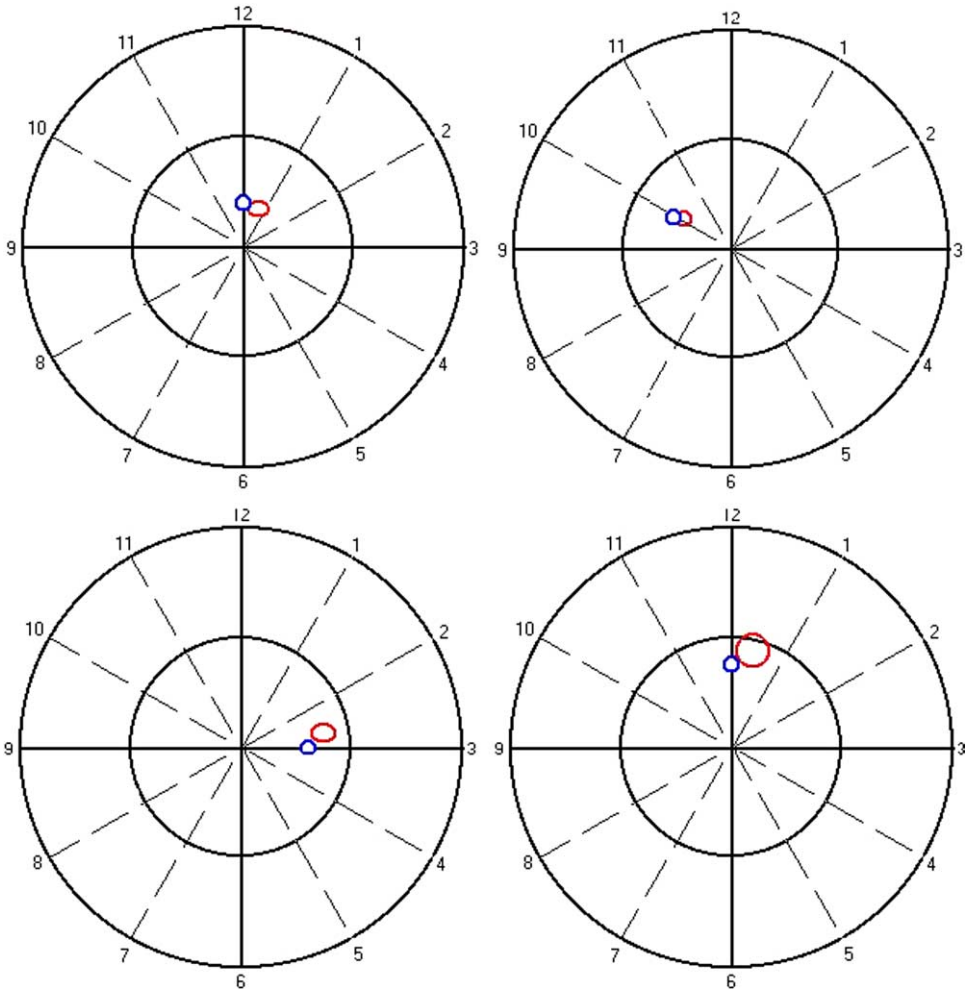

Fig. 6. Quadrant images used to evaluate the reconstructed locations of the microcalcifications from MPGS and the locations of the microcalcifications from ultrasound scanning. The red circle presents the location of the reconstructed microcalcifications, and the blue circle presents the locations of the microcalcifications from ultrasound scanning (For interpretation of the reference to color in this legend, the reader is referred to the web version of this article).

After obtaining the 3D microcalcifications, these 3D microcalcifications were augmented on the real human body model in 3D space to show the radiologists the relative positions in the breast. In our experiments, the human body model was reconstructed from eight images surrounding the patient, each with 45°. The projection contours of the reconstructed 3D human breast model were used in rectifying the locations of the microcalcifications. After rectification, the reconstructed 3D microcalcifications were augmented on the 3D human model to present their relative locations in the human breast according to the nipple position. We set 3D human body model as the model shape and reconstructed microcalcifications models as data shape. Then based on the location of the nipple, these two models

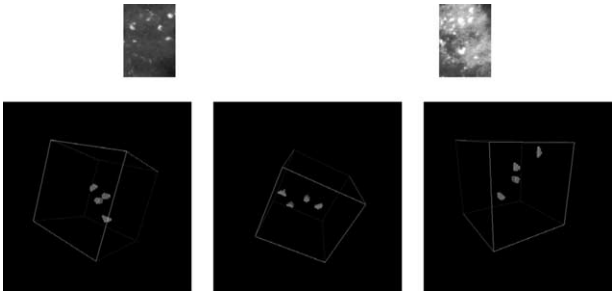

Fig. 7. Three-dimensional reconstruction of microcalcifications from CC and MLO views. The gray spheres represent the vertices of the microcalcifications in the 3D space.

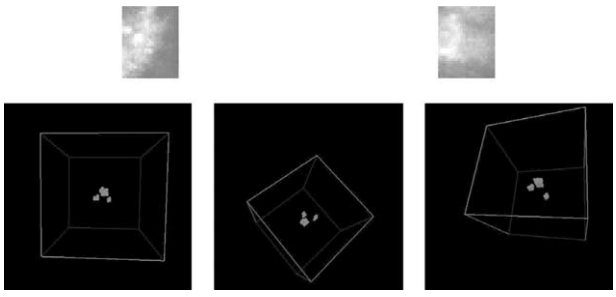

Fig. 8. Three-dimensional reconstruction of microcalcifications from its CC and MLO views. The gray spheres represent the vertices of the microcalcifications in the 3D space.

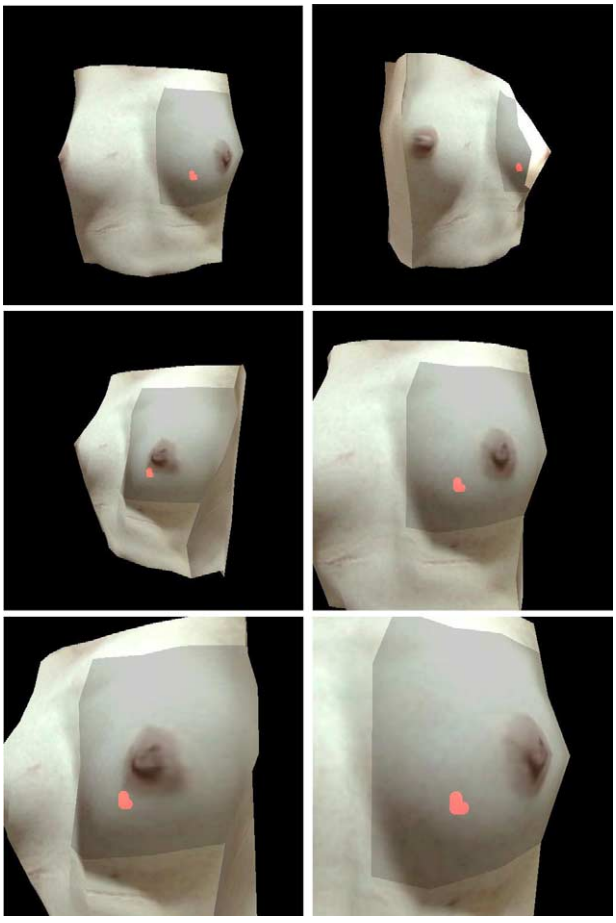

Fig. 9. Microcalcifications rendered on real human body model.

can be composed using ICP algorithm. The overlay results of 3D reconstructed clustered microcalcifications and the human body model are shown in Fig. 9, where the red volumes are the reconstructed 3D clustered microcalcifications. Since the microcalcifications are located inside the breast, the texture of the human body model in Fig. 9 is set to partially transparent to show the relative locations of them. Note that the un-smoothed texture in human body model is due to the light effects of the different images.

7. Conclusions

In this paper, a MPGS scheme is proposed to reconstruct the 3D locations of microcalcifications from two mammograms. The MPGS defines a unique space using corresponding points and the epipoles retrieved from the fundamental matrix of the CC and MLO views, to depict the reconstructed microcalcifications. Considering that the microcalcifications have been under compression, a real human body model is also reconstructed by the MPGS combined with ICP (MPGS–ICP algorithm) and used as a reference of uncompressed breast model to rectify the positions of the microcalcifications. The rectification is conducted through the concept of the bundle adjustment by minimizing the distance between the breast contours of the real human breast model and those obtained from the mammograms. With this approach, the shape of the microcalcifications could also be reconstructed, by projecting the neighboring vertices of the center of the microcalcifications. Currently, we have proposed automatic detection, registration, and reconstruction of the microcalcifications from mammograms. Nevertheless, to avoid the misalignment of the corresponding microcalcifications, the radiologists can also manually select and refine the results provided by the system. Although the developed technique is still in an early stage, it has potential to be applied to clinical trials.

References

[1] Niklason LT, Christian BT, Niklason LE, Kopans DB, Slanetz PJ, Castleberry DE, et al., Digital breast tomosynthesis: potentially a new method for breast cancer screening. In: Proceedings of fourth international workshop digital mammography. Nijmegen: The Netherlands; 1998. p. 51–6.
[2] Maidment AD, Conant EF, Feig SA, Piccoli CW, Albert M. 3-dimension analysis of breast calcifications. In: Proceedings of third international workshop digital mammography. Chicago, IL; 1996. p. 245–50.
[3] Yam M, Brady M, Highnam R, Behrenbruch C, English R, Kita Y. Three-dimensional reconstruction of microcalcification clusters from two mammographic views. IEEE Trans Med Imag 2001;20:479–89.
[4] Huang C-R, Lee T-Y, Chung P-C, Lee S-K. 3-D reconstruction and rendering of mircocalcifications from two x-ray mammograms. In: Proceedings of comput graphics workshop, Taiwan, 2002.
[5] Saito H, Kanade T. Shape reconstruction in projective grid space from large number of images. In: Proceedings of IEEE computer society conference on computer vision and pattern recognition, vol. 2; 1999.
[6] Klette R, Karsten S, Andreas K. Computer vision: three-dimensional data from images. Berlin: Springer; 1998.
[7] Luong Q-T, Faugeras OD. The fundamental matrix: theory, algorithm, and stability analysis, INRIA research report 2004; 1993.
[8] Zhang Z. Determining the epipolar geometry and its uncertainly: a review, INRIA research report 2927; 1996.
[9] Arun KS, Huang TS, Blostein SD. Least-squares fitting of two 3-D point sets. IEEE Trans Pattern Anal Mach Intell 1987;9:698–700.
[10] Besl PJ, McKay ND. A method for registration of 3-D shapes. IEEE Trans Pattern Anal Mach Intell 1992;14:239–56.
[11] Lee BU, Kim CM, Park RH. An orientation reliability matrix for iterative closest point algorithm. IEEE Trans Pattern Anal Mach Intell 2000;22:1205–8.
[12] Kegelmeyer MP, Pruneda JM, Bourland PD, Hillis A, Riggs MW, Nipper ML. Computer-aided mammographic screening for spiculated lesions. Radiology 1994;191:331–7.
[13] Dengler J, Behrens J, Desaga JF. Segmentation of microcalcifications in mammograms. IEEE Trans Med Imag 1993;12:634–42.
[14] Shen L, Rangayyan RM, Desautels JEL. Application of shape analysis to mammographic calcifications. IEEE Trans Med Imag 1994;13:263–74.
[15] Laine AF, Schuler S, Fan J, Huda W. Mammographic feature enhancement by multiscale analysis. IEEE Trans Med Imag 1994;13:725–40.

[16] Netsch T, Peitgen HO. Scale-space signature for the detection of clustered microcalcifications in digital mammograms. IEEE Trans Med Imag 1999;18:774–86.
[17] Kita Y, Highnam R, Brady M. Correspondence between different view breast X-rays using a simulation of breast deformation. In: Proceedings of IEEE computer society conference on computer vision and pattern recognition; 1998. p. 700–7.
[18] Lo CS. Computer-aided system for diagnosis of clustered microcalcifications in mammograms. PhD Thesis; 2000.
[19] Liao PS, Hsu BC, Lo CS, Chung PC, Chen TS, Lee SK, et al. Automatic detection of microcalcifications in digital mammograms by entropy thresholding. In: Proceedings of 18th annual international conference of the IEEE, vol. 3; 1997. p. 1075–6.
[20] Chung PC. An algorithm for detection and segmentation of clustered microcalcifications on mammograms. In: Proceedings of second medical engineering week of the world; 1996. p. 102.
[21] Hsu BC, Chung PC, Chang CI. Automated system for detection and classification of microcalcifications in digital mammograms. In: Proceedings CVGIP'96; 1996. p. 127–34.
[22] Mandelbrot BB. The fractal geometry of nature. New York: Freeman; 1977.
[23] Pleg S, Naor J, Hartley R, Avnit D. Mutiple resolution texture analysis and classification. IEEE Trans Pattern Anal Mach Intell 1984;6:518–23.
[24] Chang C-I, Chen K, Wang J, Althouse MLG. A relative entropy approach to image thresholding. Pattern Recogn 1994;27:1275–89.
[25] Yang C-W, Chung P-C, Chang C-I, Wang J, Althouse MLG. Entropic and relative entropic thresholding. In: Proceedings of joint Conference 1996 international computer symposium; 1996. p. 82–9.
[26] Lee SK, Yang SC, Chung PC, Lo CS, Yang CW, Lee T, et al. A computer-aided diagnostic system for detection and segmentation of clustered microcalcification in digital mammograms. Chin J Rad 2001;26:107–18.
[27] Otsu N. A threshold selection method from gray-level histograms. IEEE Trans Syst Man Cybern 1979;9:62–6.
[29] Triggs B, McLauchlan P, Hartley R, Fitzgibbon A. Bundle adjustment—a modern synthesis. Vis Algorithms Theor Pract 2000;298–372.
[30] Bartoli A, Sturm P. Three New Algorithms for Projective bundle adjustment with minimal parameters, INRIA techniques report. 4236; 2001.
[31] Press WH, Teukolsky SA, Vetterling WT, Flannery BP. Numerical recipes in C. Cambridge: Cambriage University Press; 1992.
[32] Hackshaw A-K, Wald N-J, Michell M-J, Field S, Wilson A-R. An investigation into why two-view mammography is better than one-view in breast cancer screening. Clin Radiol 2000;55:454–8.